

CHARACTERIZATION OF THE SECOND PARCEL OF THE ALTERNATIVE BUFFER MATERIAL (ABM) EXPERIMENT – I MINERALOGICAL REACTIONS

S. KAUFHOLD^{1,*}, R. DOHRMANN^{1,2}, N. GÖTZE², AND D. SVENSSON³

¹BGR, Bundesanstalt für Geowissenschaften und Rohstoffe, Stilleweg 2, D-30655 Hannover, Germany

²LBEG, Landesamt für Bergbau, Energie und Geologie, Stilleweg 2, D-30655 Hannover, Germany

³Swedish Nuclear Fuel and Waste Management Co (SKB), Pl 300, SE-57295 Figeholm, Sweden

Abstract—The performance of bentonite barriers for high level radioactive waste (HLRW) disposal is currently being tested in various real- and up-scale disposal tests. One of the disposal tests, the ABM test (ABM = alternative buffer material), was conducted by SKB (Svensk Kärnbränslehantering) as a medium-scale experiment at the Äspö hard rock laboratory in Sweden. The present study deals with the second parcel (ABM-II), which was retrieved after 6.5 years with 2.5 years of water saturation and 3–4 years of heating up to 141°C. Nine different bentonites and two marine clays were tested to investigate the performance. The aim of the study was to provide a detailed characterization of the mineralogical and chemical changes that took place in ABM-II, compare the findings with ABM-I (the first of the six test parcels), and try to draw some general conclusions concerning the use of bentonites in such geotechnical barriers. The ABM-II test parcel revealed a set of reactions that a HLRW bentonite might undergo. The most prominent reaction was the rather complete exchange of cations, which was discussed in a second part to this publication (II – cation exchange; Dohrmann and Kaufhold, 2017). The corrosion of the Fe in metal canisters was observed, but no discrete corrosion product was identified. At the interface of bentonite and the metal canister, the formation of smectite-type trioctahedral clay minerals was observed. In contrast to the ABM-I test, anhydrite was present in many of the bentonite blocks of the ABM-II test. In most concepts used for HLRW disposal in crystalline rocks, a temperature below 100°C at the canister surface was applied to avoid boiling. In the ABM-II test, boiling of water was possibly observed. Throughout the experiment, a pressure/water loss was recorded in the upper part of the geotechnical barrier and water was added to maintain pressure in the bentonite. As a result of evaporation, NaCl crusts might have formed and the barrier was partly disintegrated. These results demonstrated that a reasonable assumption is that no boiling of water occurs in disposal concepts in which a pressure loss can occur.

Key Words—Buffer Material, Engineered Barrier, Geotechnical Barrier, Hard Rock Laboratory, HLRW-bentonite, *In situ* Test.

INTRODUCTION

Bentonites are planned to be used in some concepts for the disposal of high level radioactive waste (HLRW). In many HLRW disposal concepts worldwide, bentonites are planned to be used as a so called geotechnical barrier that directly surrounds the metal canisters which contain the waste. The bentonites should isolate the waste from the surrounding host rock mainly through the low hydraulic permeability, the adsorption of hazardous radionuclides, and the sealing of any cracks in the barrier by the extraordinary swelling capacity of bentonites (Dohrmann *et al.*, 2013a). Details on the use of bentonite as a HLRW barrier material were given by Pusch *et al.* (1995), Mosser-Ruck *et al.* (2001), Wilson *et al.* (2006a, 2006b), Sellin and Leupin (2014), and Kaufhold and Dohrmann (2016). The performance of bentonite barriers is currently tested in various real- and up-scale disposal tests and the “alternative buffer material, ABM” test is one of those disposal tests. The

ABM test was described in detail by Eng *et al.* (2007) and Svensson and Hansen (2013). In the frame of the ABM tests, nine different bentonites and two marine clays are tested within one experiment to identify performance differences when used as a geotechnical barrier material. The first package, named ABM-I, was retrieved in 2009 after being saturated with water and heated for more than one year. Details about the test and the results were published by Svensson *et al.* (2011), Kumpulainen and Kiviranta (2011), Kaufhold *et al.* (2013), and Dohrmann *et al.* (2013b). Most of the results published in the aforementioned studies were obtained by the investigation of only a few blocks. The following different mineralogical reactions were identified which need to be investigated further: (1) The Fe-content increased at the contact due to Fe-corrosion of the metal canister; (2) the Mg-content increased at the contact probably from the combined effects of the formation of trioctahedral clay minerals; (3) the dissolution and precipitation of carbonates and/or sulfates; (4) organics at the heater contact were enriched due to a lubricant that was added during block fabrication; and (5) cristobalite and zeolite were dissolved (Kaufhold *et al.*, 2013; Wersin *et al.*, 2015). In addition, the

* E-mail address of corresponding author:

s.kaufhold@bgr.de

DOI: 10.1346/CCMN.2016.064047

distribution of exchangeable cations in smectite interlayers almost completely equilibrated with the surrounding water (Dohrmann *et al.*, 2013b) which was confirmed by modeling (Wallis *et al.*, 2016).

After water saturation for approximately 2.5 years followed by 3–4 years of heating, ABM-II was retrieved in 2013. Because the heating phase was longer in ABM-II than in ABM-I, the reactions identified in ABM-I should be more pronounced in ABM-II. Kumpulainen *et al.* (2016) studied four out of thirty-one compacted bentonite blocks made of MX80, Deponit CAN, and Friedland clay (FRI) in the lower part of the ABM-II parcel (blocks 2, 4–6). In the bentonite blocks, different cation exchange processes were identified by these authors as well as the accumulation of water soluble SO_4 , a decrease in the content of poorly crystalline iron oxides, the accumulation of Mg, Ca, S, and a decrease in Na and K contents with increased distance away from the heater towards the rock. Directly at the heater contact, Fe accumulated, Si and Al contents decreased, gypsum and anhydrite were precipitated, cristobalite and feldspars were dissolved, and indications for the formation of trioctahedral clay minerals were found. Kumpulainen *et al.* (2016) also observed an increase in exchangeable Ca^{2+} and a decrease in exchangeable Na^+ , Mg^{2+} , and K^+ . The CEC, however, did not change. Svensson (2013) identified a trioctahedral smectite in block 9 (Febex). Kaufhold *et al.* (2013) also studied only a few buffer blocks for the mineralogical and geochemical characterization of the ABM-I test. The results of ABM-I investigations, however, showed that all blocks should be investigated to better understand the equilibrium conditions in the whole test parcel. To properly characterize the reactions that took place in the ABM-II test, all blocks were sampled.

The aim of the present study was to provide a detailed characterization of the mineralogical and chemical changes that took place in the ABM-II test, compare the findings with the ABM-I test results, and try to draw some general conclusions concerning the performance of bentonites in geotechnical barriers for the safe disposal of HLRW.

MATERIALS AND METHODS

In the ABM test conducted in the Äspö hard rock laboratory, a 108 mm diameter iron tube with a heater system inside was surrounded by different blocks of the compacted and commercially mined bentonites. The samples were denoted/abbreviated (origin) as follows: MX80 (Wyoming, USA), Kunigel V1 (JNB, Tsukinuno, Japan), Calcigel (CAL, Bavaria, Germany), Ibeco Seal M-90 (IBE, Askana, Georgia/CIS), Febex (Almeria, Spain), Ikosorb (IKO, Mount Tidienit, Morocco), Rokle (Czech Republic), Asha 505 (Kutch, India), and Deponit CAN (Dep. CAN, Milos, Greece). The marine clays Friedland (Neubrandenburg, Germany) and

Callovo-Oxfordian (COX, Meuse/Haute-Marne, France) were also used.

The outer diameter of the individual blocks was 280 mm, the inner diameter was 110 mm, and the height was 100 mm. A package of 31 blocks was placed vertically in the Äspö crystalline rock (granite). The heating period of the first three out of six packages started in 2005, but note that the sequence of clay types in the different packages differed (Eng *et al.*, 2007). In 2012, three additional packages of bentonite blocks were prepared and heating was started. Any significant conclusions which can be drawn from the ABM tests have to be independent of the bentonite sequence. The different bentonite sequences, however, complicate comparisons between the different packages.

Most of the samples could be retrieved either as one piece or as a few pieces with clearly observable interfaces (both bentonite to sand/crystalline rock or to the heater). In some areas, however, some sample pieces were retrieved which could not be sampled in a laboratory because the interfaces could not be identified. In this region, boiling of water was suspected that was possibly the result of local pressure relief.

Sampling of the blocks was conducted as described by Kaufhold *et al.* (2013; Figure 1) in which the “0.1-cm sample” was collected by scratching off approximately 2 g from the contact surface and 2-g samples at 2, 5, and 8 cm distances from the contact were collected by drilling 1 cm diameter holes about 3 cm deep in the blocks with a hand auger. Three holes in the bentonite blocks were drilled to different vertical depths and all the material removed from the holes was mixed together. Any possible vertical gradients in bentonite block composition could not, therefore, be investigated based on this sample set (Table 1). According to Kaufhold *et al.* (2013) and Dohrmann *et al.* (2013b) vertical gradients were assumed to be low. The excavation of the ABM experiment could not be performed in an O_2 -free atmosphere. Accordingly, no glove box was used in the laboratory. The actual temperature measured at three different distances from the heater (Figure 2) ranged from 120–140°C at the heater and from 86–102°C 6 cm away from the heater. All samples were investigated to identify any chemical or mineralogical changes using appropriate established methods. For the X-ray fluorescence (XRF) analyses of powdered samples, a PANalytical Axios spectrometer was used (PANalytical, Almelo, The Netherlands). Samples were prepared by mixing with a flux material (lithium metaborate Spectroflux, Flux No. 100A, Alfa Aesar) and was melted into glass beads. The LiBO_2 beads were analyzed using wavelength-dispersive XRF. To determine the loss on ignition (LOI), 1000 mg of sample material were heated to 1030°C for 10 min.

X-ray diffraction (XRD) patterns were recorded using a PANalytical X'Pert PRO MPD θ - θ diffractometer (PANalytical, Almelo, The Netherlands) using $\text{CuK}\alpha$ radiation generated at 40 kV and 30 mA. The XRD was

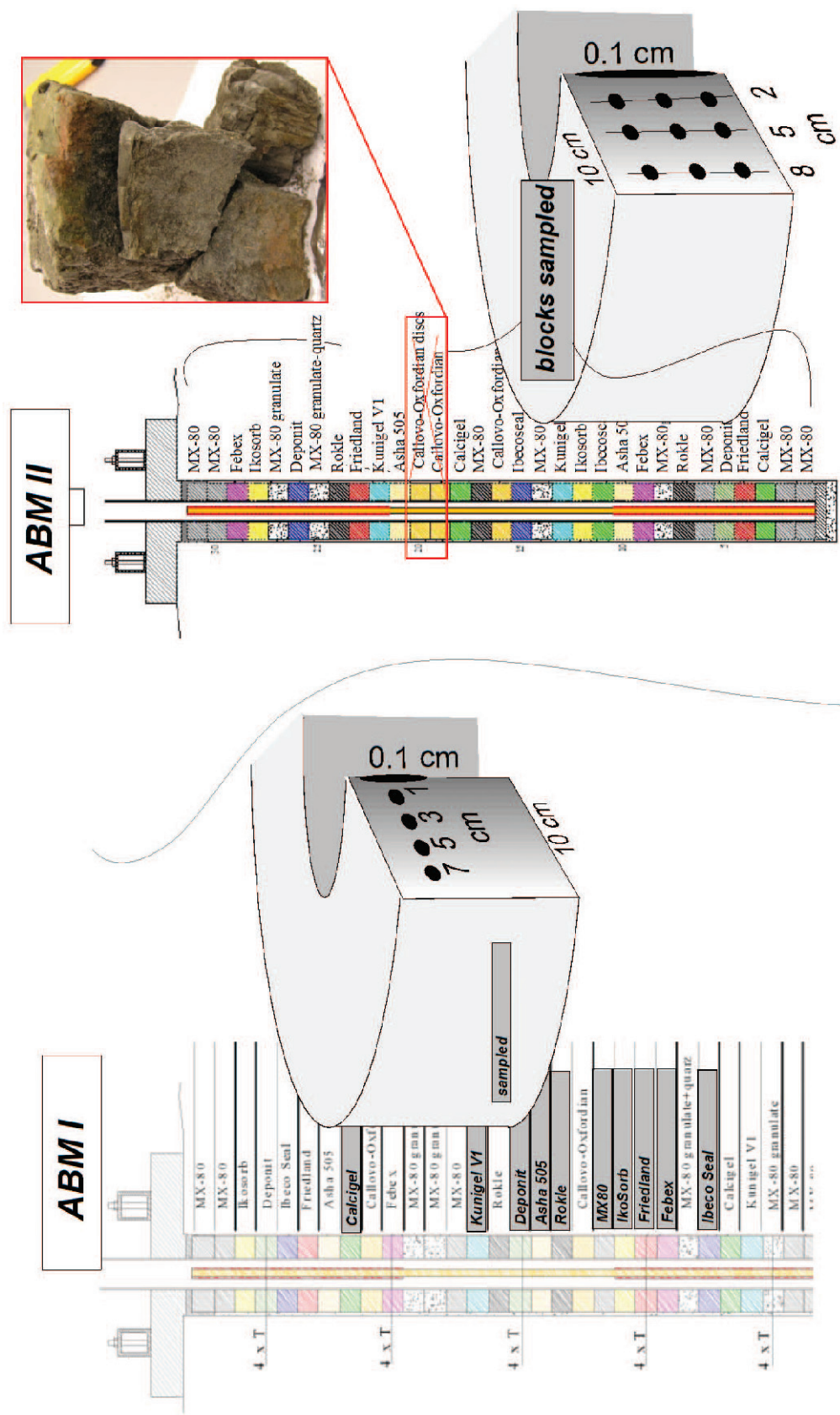


Figure 1. Experimental setup and sampling strategy for the ABM I (left, Kaufhold *et al.*, 2013) and ABM II test (right, this study).

Table 1. List of all samples collected from the ABM-II retrieved bentonite blocks and photographs of some blocks showing the integrity of the material after retrieval.

Block	Material/abbreviation	1 mm	2 cm	5 cm	8 cm
31	MX80	x	x	x	x
30	MX80	x	x	x	x
29	Febex	x	x	x	x
28	Ikosorb (IKO)	x	x	x	x
27	MX80 granulate	x	x	x	x
26	Dep. CAN	x	x	x	x
25	MX80 granulate +quartz	x	x	x	x
24	Rokle (Rawra)	x	x	x	x
23	Friedland (FRI)	x	x	x	x
22	Kunigel V1 (JNB)	x	x	x	x
21	Asha 505	x	x	x	x
20	Callovo-Oxfordian				
19	Callovo-Oxfordian				
18	Calcigel (CAL)	x	x	x	x
17	MX80	x	x	x	x
16	Callovo-Oxfordian	x	x	x	x
15	Ibeco Seal (IBE)	x	x	x	x
14	MX80 granulate +quartz	x	x	x	x
13	Kunigel V1 (JNB)	x	x	x	x
12	Ikosorb (IKO)	x	x	x	x
11	Ibeco Seal (IBE)	x	x	x	x
10	Asha 505	x	x	x	x
9	Febex	x	x	x	x
8	MX80 granulate	x	x	x	x
7	Rokle (Rawra)	x	x	x	x
6	MX80	x	x	x	x
5	Dep. CAN	x	x	x	x
4	Friedland (FRI)	x	x	x	x
3	Calcigel (CAL)	x	x	x	x
2	MX80	x	x	x	x
1	MX80	x	x	x	x

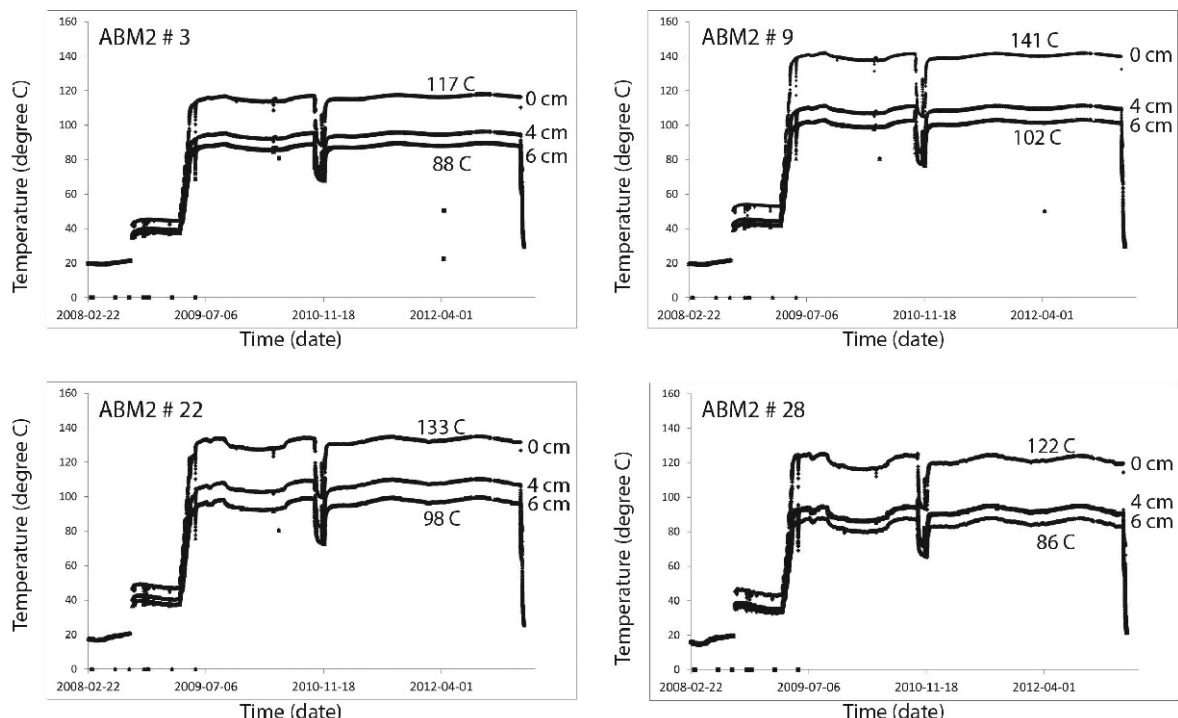


Figure 2. Temperature distribution at 0, 4, and 6 cm from the heater T sensors in block 3 (upper left), block 9 (upper right), block 22 (lower left), and block 28 (lower right).

equipped with a variable divergence slit (20 mm irradiated length), primary and secondary soller slits, proportional counter, a secondary monochromator, and a sample changer (sample diameter 28 mm). For random powder mount specimen preparation, the side loading technique was used. The samples were scanned from 2° to $90^\circ 2\theta$ with a step size of $0.02^\circ 2\theta$ and a measuring time of 20 s per step. The measuring time varied between 1 and 10 s per step. Oven-dried clay fractions $<2 \mu\text{m}$ were dispersed using ultrasound. Suspensions were transferred to 27 mm diameter ceramic tiles using a vacuum filter in order to preferentially orient the clay minerals (phyllosilicates) parallel to the basal planes. Different conditions were applied for qualitative analysis: (1) air-dry (AD) and (2) ethylene glycol (EG) solvated. The oriented mounts were scanned from 2° to $35^\circ 2\theta$ with a step size of $0.02^\circ 2\theta$.

Thermoanalytical investigations were performed using a Netzsch 449 F3 Jupiter thermobalance (Netzsch, Selb, Germany) equipped with a differential scanning calorimeter/thermogravimetric analyser (DSC/TG) and sample holder linked to a Netzsch QMS 403 C Aeolus mass spectrometer (MS) (Netzsch, Selb, Germany). Samples of 100 mg powdered material that was previously equilibrated at 53% relative humidity (RH) were heated from 25–1150°C with a heating rate of 10 K/min. For measuring the mid (MIR) infrared spectra, the KBr pellet technique (1 mg sample/200 mg KBr) was applied. Spectra were collected on a Thermo Nicolet Nexus Fourier-transform infrared (FTIR) spectrometer (ThermoFisher Scientific, Waltham, Massachusetts, USA). The FTIR had a MIR beam splitter, a KBr window, a DTGS TEC detector, and the resolution was adjusted to 2 cm^{-1} . The FTIR measurements were conducted before and after the pellets were dried at 150°C in a vacuum oven for 24 h. Total carbon (TC), total organic carbon (TOC), total inorganic carbon (TIC), and total sulfur (S) contents were determined using a LECO CS-444 analyzer (LECO Corporation, St. Joseph, Michigan, USA) by heating powdered samples to 1800–2000°C in an oxygen atmosphere. Evolved gaseous products were detected by infrared absorption and were quantified by comparison with standards. After the TC determination, samples were measured again after carbonate dissolution which was performed several times at 80°C using HCl until no further gas evolution was observed to give the TOC content. The TIC was calculated by the difference between the TC and TOC values. The error in the LECO values in the present study was $<0.1 \text{ mass}\%$.

For scanning electron microscopy (SEM) investigations, a FEI Quanta 600 F (FEI/ThermoFisher Scientific, Eindhoven, The Netherlands) was used and was operated in low-vacuum mode (0.6 mbar). Sputter coating the samples with gold or carbon, therefore, was not necessary. The microscope was equipped with an EDX-system Genesis 4000 (EDAX, Inc., Mahwah,

New Jersey, USA) for energy dispersive spectroscopy. Freshly broken surfaces of unprocessed pieces of bentonite blocks were investigated using SEM after the samples were slowly air dried. Suspensions of the bentonite samples were produced by dispersing 1 g of the solid in 50 mL of water (2% suspension) and the pH value was measured using a standard pH electrode (Kaufhold *et al.*, 2008).

RESULTS AND DISCUSSION

The chemical compositions and other basic geochemical data of all of the samples including reference materials (REF) in Supplemental Materials section (Table 2, deposited with the Editor-in-Chief and available at <http://www.clays.org/JOURNAL/JournalDeposits.html>) revealed that changes in the chemical compositions reflected different reactions, which are discussed below. The exchangeable cation and CEC data will be discussed in the second part of the publication (Dohrmann and Kaufhold, 2017). Notably, only those values which showed significant changes were given. As an example, trace elements other than those given in Table 2 (As, Ba, Bi, Ce, Co, Cs, Cu, Ga, Hf, La, Nb, Nd, Pb, Rb, Sb, Sc, Sm, Sn, Ta, Th, U, V, W, Y, Zr) did not reveal significant differences and, hence, are not shown.

Corrosion

The ABM-II package was equipped with a steel pipe made of common carbon steel, P235TR1, which was used to house the heaters. The ABM-II package was also equipped with sensors, a saturation system, and granulate cages (black steel frame wrapped with a fiber cloth). All these metallic materials in the ABM-II package could have been corroded during treatment, which might have influenced composition of the bentonites. Thermocouple sensors with shields of cupronickel were mounted at five levels in the package on block numbers 3, 9, 15, 22, and 28, but did not contact the bentonite-canister interface. Relative humidity sensors were positioned in the same blocks, but were positioned in holes in the inner parts of the blocks at a distance of 3 cm from the heater-bentonite interface. The saturation system was made using perforated Ti pipes which supplied the blocks with groundwater at the outer part of the blocks at the contact with crystalline rock. No influence of the sensors and the Ti pipes on the chemical composition of the heater-bentonite interface was expected (Grolimund *et al.*, 2016). The granulate cages, however, consisted of a black steel frame wrapped with a fiber cloth. These cages positioned at blocks No. 8, 14, 25, and 27 were in contact with the heater (see Figure 3 which shows parts of a cage after retrieval). Iron is known to corrode in contact with bentonite. In a first corrosion step, the entrapped oxygen is consumed and results in red and/or black halos. Most of the iron, however, reacts under anaerobic conditions



Figure 3. Block 27 and black steel cage with MX80 granulate material after retrieval.

(*e.g.* Samper *et al.*, 2016). The neo-formation of iron-silicates (such as berthierine or chlorite, Lantenois *et al.*, 2005, Osacký *et al.*, 2010, Kaufhold *et al.*, 2015) was observed in laboratory experiments. Kumpulainen *et al.* (2016) did not identify any neo-formed Fe-bearing mineral phases in the lower part of the ABM-II parcel (blocks 2, 4-6), the content of Fe-bearing mineral phases did not increase, and no changes in the smectite composition was observed (*i.e.* Fe content). No sign of the corrosion products commonly observed in the laboratory (*e.g.* berthierine) was found. No neo-formed Fe-silicates were detected by XRD, which is in accordance with Kumpulainen *et al.* (2016). Differential thermal analysis-mass spectrometry (DTA-MS) using the Aeolus MS, on the other hand, indicated traces of siderite. For four samples (all MX80 blocks 8, 17, 30, and 31), a small peak in the CO₂-mass spectrometer curve between 500 and 600°C was observed and indicated the presence of small amounts of siderite (which typically decomposes at a relatively low temperature). The assumed siderite DTA-MS signal, however, was weak and suggests that the siderite concentration was low and much below the XRD detection limit. Corrosion was mostly reflected by the increased Fe-contents in the 1-mm samples, which were collected at the heater/bentonite contacts. As in ABM-I, different increases in Fe content were observed, which may depend on the type of bentonite. An increase in the Fe-content (+Fe₂O₃ in mass%) was used to indicate the extent of corrosion (Table 3). These results do not provide a general correlation, but revealed some trends. The Fe-increase was relatively high for all MX80 samples (+2 to +5 mass%). The increase was more or less the same and ranged from +3 to +5 mass% Fe₂O₃ for the granulate cages of MX80 at block positions 8, 14, 25, and 27. The neighboring blocks did not show a

significant Fe increase. The non-granular MX80 blocks (1, 2, 6, 17, 30, and 31) showed slightly lower Fe increases (+2 to +4 mass% Fe₂O₃). All Deponit CAN, CAL, ROK, and FRI samples had less of an increase in Fe. Samples ASHA 505 (+1 to +5 mass% Fe₂O₃), IBE (+2 and +8 mass% Fe₂O₃), and JNB (+1 and +4 mass% Fe₂O₃) were different. The reason for the comparably large Fe corrosion at contacts with the MX80 samples might be due to the low layer charge density (Kaufhold *et al.*, 2015) and different local conditions might explain the other observed differences. The Ni contents of the reference (REF) samples ranged from <2 to 89 mg/kg. Some samples showed a Ni content increase of up to +45 mg/kg in the 1-mm samples from the heater contact. The measured Ni could have been derived from the Fe heater or from the black steel cage frame used for the four MX80 granulate or “granulate + quartz” blocks, but correlations between the Ni and Fe₂O₃ increases were poor. Apart from a general trend, some samples showed a high Ni increase but a low Fe₂O₃ increase (*e.g.* blocks 4 and 14). The Ni could also be derived from the sensors or other metal devices used to setup the test. The Ni-source, therefore, has not yet been identified. Corrosion was further investigated using electron microscopy. For electron microscopy using EDX, all the bentonite blocks were freshly broken (*i.e.* to avoid artifacts) and slowly dried and included samples from the metal contact. Note that the electron microscopy EDX samples were subjected to oxygen during drying. Micrographs selected to represent the observations made on all the blocks (Figure 4) revealed that the contact area of block 4 contained a layer of gypsum crystals that was larger than 50 μm (Figure 4 inset, B04). The total S concentrations in block 4 did not change, but a marked difference in the SO₃-content (XRF) of the 1-mm sample was observed (Table 2) in comparison with the reference and can be

Table 3. The increased Fe content, Fe-phases, and increased Ni in the 1-mm samples, bold = significant changes, italics = no significant changes.

Block		Fe ₂ O ₃ increase $\Delta_{\text{after-before}}$ (mass%)	Fe-phases	Ni increase $\Delta_{\text{after-before}}$ (mg/kg)
31	MX80	4	STA: sid?	5
30	MX80	4	STA: sid?	1
29	Febex	2		-1
28	Ikosorb (IKO)	2		0
27 cage	MX80 granulate	4		3
26	Dep. CAN	2		-6
25 cage	MX80 gran+qtz	3		3
24	Rokle (Rawra)	-1		-5
23	Friedland (FRI)	0		4
22	Kunigel V1 (JNB)	1		5
21	Asha 505	1		-12
20	not sampled			
19	not sampled			
18	Calcigel (CAL)	2		1
17	MX80	5	STA: sid?	0
16	Callovo-Oxfordian	8		24
15	Ibeco Seal (IBE)	8		0
14 cage	MX80 gran+qtz	3		35
13	Kunigel V1 (JNB)	4		8
12	Ikosorb (IKO)	4		8
11	Ibeco Seal (IBE)	2		2
10	Asha 505	5		5
9	Febex	3		-3
8 cage	MX80 granulate	5	STA: sid?	0
7	Rokle (Rawra)	1		1
6	MX80	3		7
5	Dep. CAN	1		0
4	Friedland (FRI)	0		45
3	Calcigel (CAL)	1		3
2	MX80	3		10
1	MX80	2		3

explained by the oxidation of an Fe-sulfide that was initially present. Throughout the production of the XRF glass beads, sulfide was largely oxidized and did not contribute to the SO₃-values, whereas the sulfates are decomposed at much higher temperatures and, hence, sulfates mostly persisted in the beads. This explains the difference in S values in the LECO and XRF analyses. Several EDX-line scans were recorded from a distance of about 0.5 mm (example shown in Figure 4, B07, Rokle). The bentonite heterogeneity, however, was more significant than the bulk chemical gradients in the drilled samples. The EDX analyses, therefore, did not provide additional information about the metal-bentonite interface. This confirmed the heterogeneity of the bentonite-canister interfaces in the prototype repository samples which had a copper heater that was observed using SEM-EDX by Dohrmann and Kaufhold (2014). The SEM images of block 24 show a heterogeneous distribution of Fe (oxyhydr)oxides and an enrichment of small Fe (oxyhydr)oxide particles near the contact (Figure 4, B24). In the marine clay sample in block 30 (Figure 4, B30), a well separated and relatively homogeneous Fe-

rich layer could be distinguished from the bentonite precursor material. The layer was about 10 µm thick and explained the marked Fe content increase in the 1 mm sample from block 30. On the other hand, no such Fe layer was found in all the other samples that had a marked increase in the Fe content. Initially, a gap of about 1 mm was observed between the blocks and the steel pipe. The role of this gap with respect to corrosion is not yet clear. At least, the gap contained oxygen which was consumed to produce the oxidic corrosion of the pipe.

Mg increase and the formation of trioctahedral clay minerals

At the contact between a heater and bentonite, a Mg increase was found in many of the large- and up-scale disposal tests in which a heater was used to create a thermal gradient (crystalline rock, LOT-experiment: Karnland *et al.*, 2009, ABM-I, Kaufhold *et al.*, 2013; prototype repository (PTR): Dohrmann and Kaufhold, 2014; clay: Mont Terri rock laboratory, Heater Experiment HE-B, Plötze *et al.*, 2007). The mechanisms involved are, however, not yet clear. Apparently, along

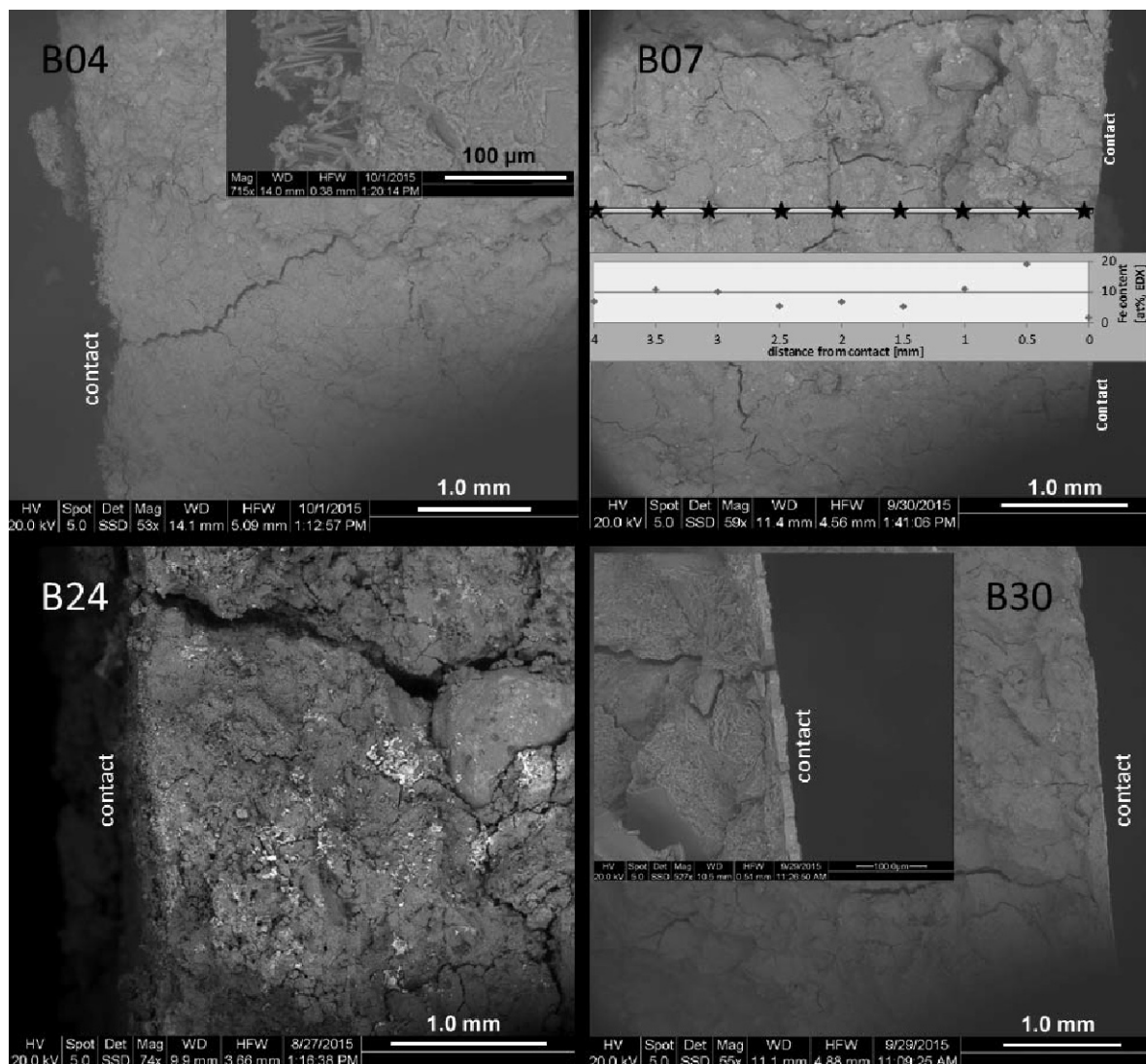


Figure 4. Selected SEM micrographs of the contacts with the iron heaters (B04 = block 4, FRI; B07 = block 7, Rokle; B24 = block 24, Rokle; B30 = block 30, MX80).

with an increase in Mg, an increase in both the IR intensity at 680 cm^{-1} and the XRD intensity at 1.53 \AA were found in ABM-I and both point toward the formation of trioctahedral domains or even a discrete saponite (Baldermann *et al.*, 2014). Svensson (2013) found an increase in the XRD intensity at 1.55 \AA (*i.e.* d_{060}) in a sample from the contact between Febex block 9 and the heater. The XRD of the EG-solvated clay sample indicated that only smectites were present in this sample. Both indicators for the possible formation of trioctahedral clay minerals were also found in some samples of the present study (Figures 5 and 6). The degree to which the formation of trioctahedral clay minerals was indicated by either IR, XRD, or the Mg increase, however, differed from one sample to another (Table 4). As an example, all trioctahedral indicators

were found at the contacts of blocks 9–11. In contrast, the d_{060} XRD reflection and the 680 cm^{-1} IR band were clearly observed at the contact of block 15, but the MgO increase was insignificant and the amount of exchangeable Mg^{2+} (Dohrmann and Kaufhold, 2016) did not change. This indicated that another explanation may exist for the MgO increase other than the formation of trioctahedral clay minerals, which could be an addition reaction with Mg^{2+} entering octahedral sheet vacancies in the simplest form. A discussion about possible mechanisms would, however, be highly speculative based on the presented data. Kaufhold *et al.* (2016), however, demonstrated that the Mg can reach the octahedral vacancies which can lead to the formation of trioctahedral domains. The dissolution of dioctahedral smectites and precipitation of trioctahedral smectites

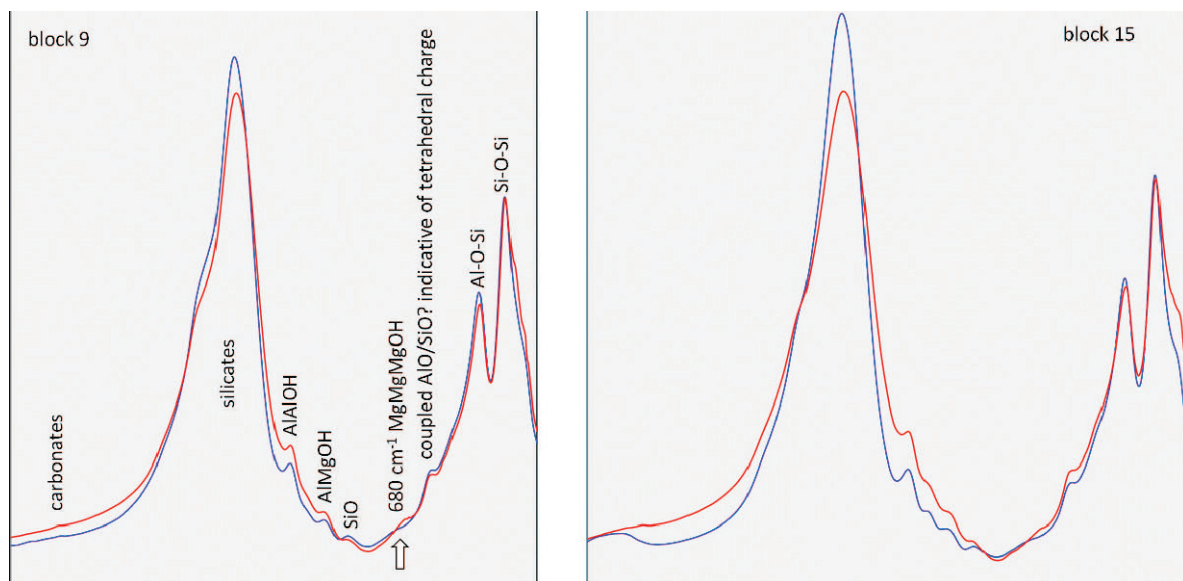


Figure 5. Examples of the increased intensity of the 680 cm^{-1} band for the 1-mm samples at heater/bentonite contact (left Febex, block 9; right IBE, block 15; blue (top spectrum) = before, red (bottom spectrum) = after).

would be an alternative reaction pathway. In addition, note that the differences between the IR and XRD patterns before and after retrieval of the bentonite blocks were too small to decide whether or not any change occurred (question marks in Table 4). The partly inconsistent picture (*i.e.*, a misfit between the different indications of trioctahedral clay mineral formation), therefore, might be due to the fact that some of the

changes were close to the detection limit. In addition, anhydrite (CaSO_4) precipitation can also lead to an increase in the intensity of the IR band at 670 cm^{-1} . The 680 cm^{-1} band cannot be assessed if anhydrite was precipitated. The new d_{060} peak in the block 9 XRD pattern was 1.53 \AA , which differs from the analysis of Svensson (2013) who found a peak at 1.55 \AA and indicated a different chemical composition (perhaps

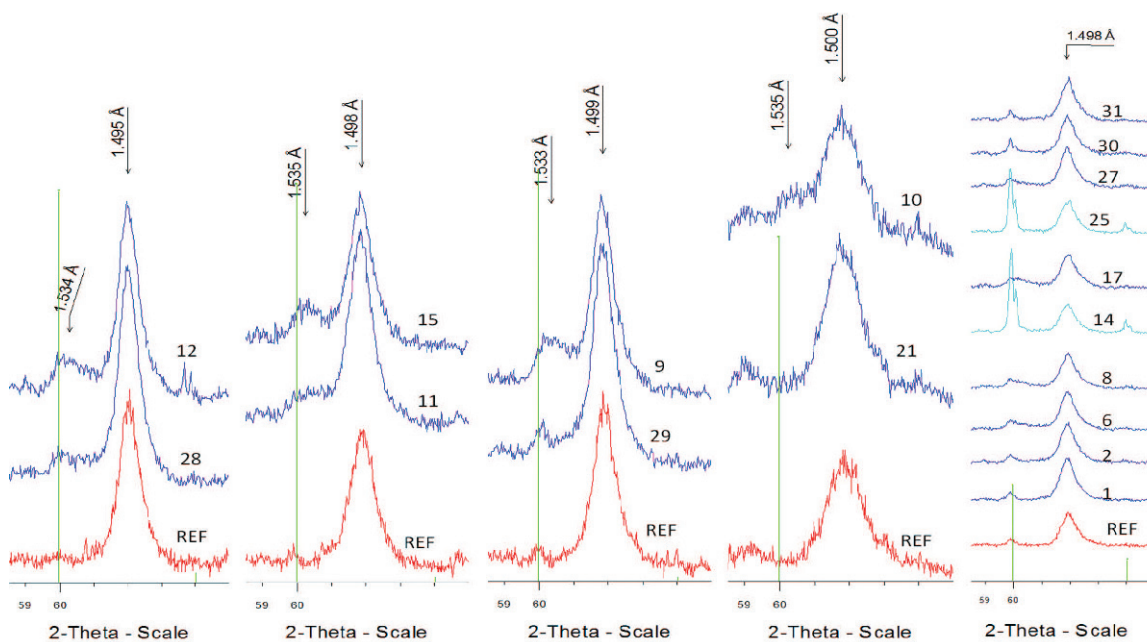


Figure 6. Examples for the increased intensity of the d_{060} peak for the 1-mm samples at the heater/bentonite contact. The green (vertical) lines in each pattern at $\sim 60^\circ 2\theta$ indicate the positions of a quartz reflection. From left to right: IKO (REF, 12, 28), IBE (REF, 11, 15), Febex (REF, 9, 29), ASHA 505 (REF, 10, 21), and MX80 (REF, 1, 2, 6, 8, 14, 17, 25, 27, 30, 31).

Table 4. The XRD and IR data for the 1-mm samples interpreted with respect to the formation of trioctahedral clay minerals. The XRD patterns of the sedimentary samples (FRI and COX) were not evaluated, bold = significant changes, italics = no significant changes.

Block		d_{060} "+" = 1.525–1.535 Å increased	+ MgO (mass%) $\Delta_{\text{after-before}}$	680 cm^{-1} "+" = band increased, "?" = possible incr.	d_{001} EG "–" no changes	free SiO_2 3740 cm^{-1} "?" possible increase
31	MX80		0.1		–	
30	MX80		–0.1		–	
29	Febex	?	0.2	?	–	
28	Ikosorb (IKO)	?	1.0		–	
27 cage	MX80 granulate		1.0		–	
26	Dep. CAN	+	1.8	?	–	
25 cage	MX80 gran+qtz		0.4		–	
24	Rokle (Rawra)		2.8	?	–	
23	Friedland (FRI)		1.9	?		
22	Kunigel V1 (JNB)		0.7		–	
21	Asha 505		–0.1		–	
20	not sampled					
19	not sampled					
18	Calcigel (CAL)	?	–0.5		–	
17	MX80		0.9		–	
16	Callovo–Oxfordian		0.2			
15	Ibeco Seal (IBE)	+	0.1	+	–	
14 cage	MX80 gran+qtz		0.1		–	
13	Kunigel V1 (JNB)		0.8		–	
12	Ikosorb (IKO)	+	0.3		–	
11	Ibeco Seal (IBE)	?	1.6	?	–	
10	Asha 505	+	2.9	?	–	
9	Febex	+	1.6	+	–	
8 cage	MX80 granulate		0.5		–	
7	Rokle (Rawra)		0.0		–	
6	MX80		1.2		–	
5	Dep. CAN		0.3		–	?
4	Friedland (FRI)		0.2			
3	Calcigel (CAL)		0.0		–	?
2	MX80		0.0		–	
1	MX80		–0.1		–	

more structural Fe) for the newly formed smectite mineral (compare to Heuser *et al.*, 2013). In the present study, the sample was taken from the surface of the bentonite block, whereas Svensson (2013) took the sample directly at the surface of the iron heater after removal of the bentonite block. Can the distance of the sample from the heater control the composition of the newly formed trioctahedral phase? Further studies are needed to clarify the nature of these differences in composition. Some mineral reactions, such as illitization (Kaufhold and Dohrmann, 2010), result in the formation of so called “free silica,” which is similar to a silica gel and, hence, is characterized by the presence of SiOH groups. These surface SiOH groups can be detected by infrared spectroscopy by examining the infrared absorption at 3740 cm^{-1} . In the ABM-I test (Kaufhold *et al.*, 2013), some samples were found with a clearly increased IR intensity in this range. In the present study, all bentonite blocks were, therefore, investigated for a

possible intensity increase in the 3740 cm^{-1} band. The heater contact samples of blocks 3 (CAL) and 5 (Dep. CAN) showed a minor increase of the 3740 cm^{-1} band, but the intensity was weak and, hence, whether or not this result was significant is questionable. In the ABM I test, free silica was unambiguously identified in the heater contact samples of a Deponit CAN and a CAL block. Not all retrieved blocks, however, produced from the CAL and Deponit CAN-bentonites showed free silica. This observation, therefore, cannot be interpreted unambiguously. The XRD analyses of the clay fractions of all the bentonites from the contact region (1 mm samples) were performed to verify if smectites became interstratified during the ABM-II test. Results indicated no interstratification of smectites for any block in comparison with the reference materials (MX80 data are shown as an example in Figure 7, Table 4). Smectites remained fully expandable (*i.e.* no illitization) and all other bentonites showed the same behavior (the 11 and

Table 5. A comparison between the parameters of the 1-mm samples that were affected by the use of Molykote as lubricant.

Block		+ Mo increase "+" > 50 mg/kg "- " only slight increase compared to the reference	+ Zn increase "+" > 200 mg/kg	+ org. increase "+" > 0.1 %
31	MX80	—	—	+
30	MX80	+—	+—	+—
29	Febex			—
28	Ikosorb (IKO)			
27 cage	MX80 granulate			
26	Dep. CAN			—
25 cage	MX80 gran+qtz			
24	Rokle (Rawra)			—
23	Friedland (FRI)			
22	Kunigel VI (JNB)		—	
21	Asha 505			—
20	not sampled			
19	not sampled			
18	Calcigel (CAL)			—
17	MX80	—		+
16	Callovo—Oxfordian	+—	+—	+—
15	Ibeco Seal (IBE)			
14 cage	MX80 gran+qtz	—		
13	Kunigel VI (JNB)	+	+	+
12	Ikosorb (IKO)	—	—	+
11	Ibeco Seal (IBE)			
10	Asha 505		—	+—
9	Febex	—	—	+—
8 cage	MX80 granulate			
7	Rokle (Rawra)	—	+	+
6	MX80	+	+	+
5	Dep. CAN		+—	+—
4	Friedland (FRI)	+—	+—	+—
3	Calcigel (CAL)		+—	+—
2	MX80	+	+	+
1	MX80	—	++	+—

12 block 1-mm samples were not analyzed because not enough material remained). The XRD patterns of the marine clay samples (FRI and COX) were not evaluated.

Trace elements and organic material

As in the ABM-I and the prototype repository experiments, the content of organic matter, Zn, and Mo increased at the contact, which can be explained by the lubricant (Molykote®BR2 plus) used in the manufacture of the blocks (Kaufhold *et al.*, 2013; Dohrmann and Kaufhold, 2014). The lubricant consists of waxes, oil, graphite, molybdenite, and Zn dialkyl dithiophosphate. A small portion of Molykote®BR2 plus was mixed with quartz to determine the relative contents of TOC, Mo, and Zn which must be known to interpret increases in these elements at the contact. A 1% TOC increase from the Molykote corresponds to 70 mg/kg Mo and 150 mg/kg Zn. The ratio of Zn/Mo is about 2 in the Molykote, but significantly different Zn/Mo ratios were found in the different contact samples, which indicates a different fate for these elements at least in some blocks (Table 2). At the heater contact of block 1, a significant

Zn increase was observed which probably cannot be explained by the Molykote only. In this block, a marked Zn increase was found even 2 cm from the heater. This was confirmed by Kumpulainen *et al.* (2016) who found even more organic carbon throughout all parts of blocks 4–6. In most of the blocks, however, either an increase in all the Molykote indicators or no increase at all was found (Table 5). Interestingly, the increase in the three Molykote indicators (TOC, Mo, Zn) was generally larger in the lower part of the experiment which might be related to the boiling of water that was suspected in the upper part of the blocks because boiling could have possibly removed the Molykote indicators.

Dissolution and precipitation

In different large- and up-scale HLRW tests, the dissolution of some minerals and re-precipitation in different areas or the precipitation of different minerals was observed. As an example in the first LOT experiment test, a redistribution of gypsum was found (Karland *et al.*, 2007). Gypsum was dissolved both at the inner and outer parts and was precipitated in the central part of the

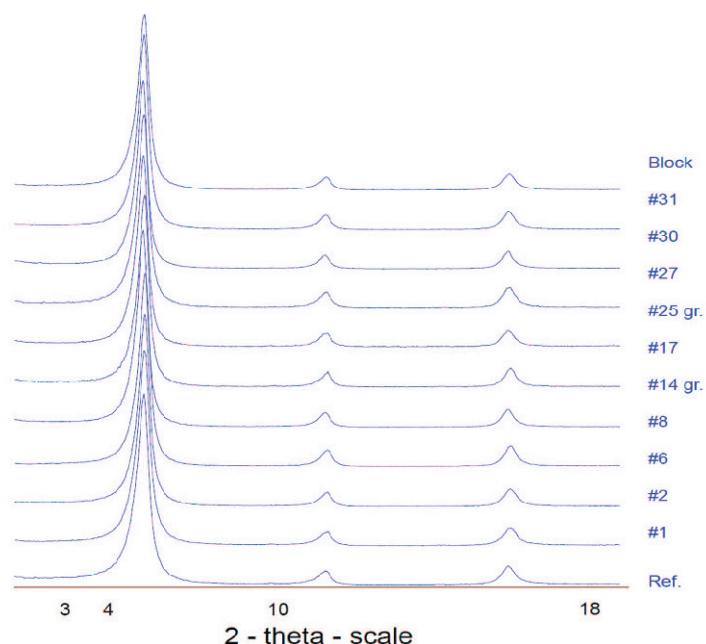


Figure 7. XRD peak positions for MX80 clay fractions of bentonites from the contact region (1-mm samples) and the REF sample after EG solvation. Granulate blocks (gr.) and granulate+quartz blocks (gr.+q) are marked.

block. In the ABM-I test, the dissolution of cristobalite and zeolite was found (Kumpulainen and Kiviranta, 2011; Kaufhold *et al.*, 2013). These non-clay minerals plus carbonates and pyrite were considered in the present study and are available in the Supplemental Materials section (Table 6, deposited with the Editor-in-Chief and available at <http://www.clays.org/JOURNAL/JournalDeposits.html>). The detection of dissolution and precipitation processes is difficult if only small concentration changes occurred. Unambiguous results were obtained using XRD which was performed on all samples. In addition, simultaneous thermal analyses (STA) and IR were performed on the 1-mm samples (Table 6). Some changes in the mineral concentrations could only be observed using STA, which is particularly sensitive to minerals that contain S and C (pyrite, gypsum, carbonates) because the masses of H₂O, CO₂, and SO₂ are detected by mass spectroscopy. In many instances, mineral changes could not be confirmed unambiguously and are indicated with a question mark in Table 6. In some contact samples, a slightly weaker XRD cristobalite peak was found which points towards the dissolution of cristobalite, but the changes were small. For example, in the case of the MX80 bentonite, the cristobalite XRD peaks were overlapped by feldspar reflections and these samples were also marked with a question mark. Note that only a few of the bentonites initially contained cristobalite. Overall, cristobalite dissolution could not be ruled out for the MX80 and IKO bentonite 1-mm samples. Gypsum was enriched at the contact in blocks 4, 16, and 23. In blocks 21 and 24, an increase in the S concentration 2 cm from the contact was found. For all MX80 samples, a

reduction in the gypsum concentration at the contact or 2–8 cm from the contact was observed (Table 6). Gypsum was almost completely preserved in the bottom (1, 2) and top (30, 31) parts of the MX80 blocks. The fate of the gypsum apparently depended on differences in the local conditions. Anhydrite precipitation was observed particularly in the upper part of the experiment (but also in block 5, Dep. CAN, compare to Kumpulainen and Kiviranta, 2011) and, hence, may be related to the assumed pressure relief. Yet explaining why anhydrite precipitation sometimes occurred at the contact and sometimes occurred ≥ 2 cm from the heater is not possible. The reason could be differences in the saturation history (Sena *et al.*, 2010). Anhydrite on the other hand, caused strongly inflated exchangeable Ca²⁺ values (Dohrmann and Kaufhold, 2016), although these authors used the Cu-trien_{5xcalcite} method which avoids errors due to soluble carbonate minerals (Dohrmann and Kaufhold, 2009). Pyrite, if it was initially present in the materials (MX80, JNB, FRI, and IBE), was dissolved in all samples but FRI. The STA-MS data indicated a small increase in the pyrite content at the contact of sample 23 (FRI). Calcite, if it was present in the starting material, was stable in all blocks of the lower part of the parcel. In the upper part, however, calcite was dissolved in many of the 1-mm samples. Only in block 16 (COX) was precipitation of calcite and dolomite detected in the entire block (as deduced from XRD and DTA-MS-CO₂ data). Again, in the lower part of the parcel, dolomite remained stable if it was initially present. Siderite was present in the REF sample of FRI and was preserved in the lower part of the parcel, whereas siderite was largely dissolved (1 mm, 2

cm, 5 cm) at block position 23 (upper part) which indicates a different geochemical milieu. Goethite was present in only two of the bentonites (Rokle and Asha 505). No changes were observed in any analyzed sample with respect to the REF samples.

Clinoptilolite dissolution may have occurred at the contact of block 13 (JNB), but the changes in XRD intensity of the most intense clinoptilolite peak were small. In contrast to the ABM-I test, halite precipitation was detected by XRD in two blocks (23 + 24). The XRF and exchangeable Na⁺ values (Dohrmann and Kaufhold, 2016), however, did not point towards significant halite, but halite XRD peaks were clearly observed.

Boiling

The blocks at positions No. 20 and 21 showed features of disintegration (Figure 8).

Apparently, boiling occurred in the warmest parts of the experiment. This was represented as an accumulation of halite near the iron heater and the corresponding blocks partially disintegrated. The temperatures were lower in the upper and lower parts of the experiment (block 3: 117°C; block 28: 122°C; Figure 2), while temperatures were higher towards the central parts (block 9: 141°C; block 22: 133°C; Figure 2). The designed maximum temperature was 130°C, but an even higher local temperature was observed (141°C). The water pressure applied was not high enough to avoid boiling at the maximum temperature observed in ABM-II. The 1.8 bar of applied pressure is enough to avoid boiling at 117°C, while 2.7 bar is needed at 130°C. This was most likely the reason for the observed boiling.

SUMMARY AND CONCLUSIONS

The ABM test revealed a set of reactions that a HLRW bentonite might undergo. The most interesting reaction was the rather complete exchange of cations

(Dohrmann and Kaufhold, 2016), which was at least partly already observed in ABM-I and will be discussed further in the second part of the publication. Secondly, some bentonites were found to be more corrosive than others (larger Fe-increase), which obviously resulted from both material properties and different local conditions. Thirdly, the formation of trioctahedral clay minerals was observed at the very contact of bentonite with the heater. Some results were close to the detection limit, but in some instances the formation of trioctahedral clay minerals was proven (as pointed out by Svensson, 2015). In the ABM-I project, the dissolution of cristobalite and zeolites was observed in some blocks. In the ABM-II tests, only few indications were found for cristobalite/zeolite dissolution. The reason for this difference is not yet understood. The most interesting information which could be gained from ABM-II is the effect of boiling because this has not been observed before. In most crystalline rock HLRW disposal concepts, a temperature below 100°C at the canister surface will be applied to avoid boiling. In the ABM-II, boiling was likely observed. Throughout the experiment a pressure/water loss was recorded in the upper part, although boiling was already suspected. As a result of the formation NaCl crusts from boiling water, exchangeable Na⁺ increased (Dohrmann and Kaufhold, 2016) and specific parts of the technical barrier disintegrated. These results demonstrate that avoiding boiling in concepts in which a pressure loss can occur is reasonable. Future studies of the other ABM packages that are still running will help to understand these processes because these bentonites have been heated even longer and the temperature was increased recently to reach approximately 160°C (or even 200°C in ABM-V). The ABM tests were designed to compare the performance of different bentonites under HLRW repository conditions. Different blocks produced from the same initial material, however, partly performed rather differently. The



Figure 8. Photograph of the fragile 19–22 bentonite blocks. Note that block 20 was constructed from two COX discs and, hence, was not very cohesive.

obtained results, therefore, indicate that different local conditions may be as important as the type of bentonite. The different local conditions, on the other hand, depend on the environment which includes the neighboring blocks. The experimental design, therefore, is not well suited to distinguish suitable from less suitable HLRW bentonites. The experiment, nevertheless, proved that mineralogical alterations were restricted to specific interfaces which did not affect the barrier performance, at least in the time frame of the experiment.

REFERENCES

- Baldermann, A., Dohrmann, R., Kaufhold, S., Nickel, C., Letofsky-Papst, I., and Dietzel, M. (2014) The Fe-Mg-saponite solid solution series – a hydrothermal synthesis study. *Clay Minerals*, **49**, 391–415.
- Dohrmann, R. and Kaufhold, S. (2009) Three new, quick CEC methods for determining the amounts of exchangeable calcium cations in calcareous clays. *Clays and Clay Minerals*, **57**, 338–352.
- Dohrmann, R. and Kaufhold, S. (2014) Cation exchange and mineral reactions observed in MX 80 buffers samples of the prototype repository *in situ* experiment in Äspö, Sweden. *Clays and Clay Minerals*, **62**, 357–373.
- Dohrmann, R. and Kaufhold S. (2017) Characterisation of the second parcel of the alternative buffer material ABM test – II Exchangeable cation population rearrangement. *Clays and Clay Minerals*, accepted.
- Dohrmann, R., Kaufhold, S., and Lundqvist, B. (2013a) The role of clays for safe storage of nuclear waste. Pp. 677–710 in: *Handbook of Clay Science, Techniques and Applications* (F. Bergaya and G. Lagaly, editors). Developments in Clay Science, Vol. **5B**, Elsevier, Amsterdam.
- Dohrmann, R., Olsson, S., Kaufhold, S., and Sellin, P. (2013b) Mineralogical investigations of the first package of the alternative buffer material test – II. Exchangeable cation population rearrangement. *Clay Minerals*, **48**, 215–233.
- Eng, A., Nilsson, U., and Svensson, D. (2007) Äspö Hard Rock Laboratory, Alternative Buffer Material Installation report IPR-07-15, 67 p., <http://skb.se/upload/publications/pdf/ipr-07-15.pdf>
- Grolmund, D., Wersin, P., Brendlé, J., Huve, J., Kiviranta, L., and Snellman, M. (2016) Interaction of titanium with smectite within the scope of a spent fuel repository: A spectroscopic approach. *Clay Minerals*, **51**, 249–266.
- Heuser, M., Andrieux, P., Petit, S., and Stanjek, H. (2013) Iron-bearing smectites: a revised relationship between structural Fe, *b* cell edge lengths and refractive indices. *Clay Minerals*, **48**, 97–103.
- Kaufhold, S. and Dohrmann, R. (2010) Stability of bentonites in salt solutions II. Potassium chloride solution – Initial step of illitization? *Applied Clay Science*, **49**, 98–107.
- Kaufhold, S. and Dohrmann, R. (2016) Assessment of parameters to distinguish suitable from less suitable high-level-radioactive waste bentonites. *Clay Minerals*, **51**, 289–302.
- Kaufhold S., Dohrmann R., Koch D., and Houben G. (2008) The pH of aqueous bentonite suspensions. *Clays and Clay Minerals*, **56**, 338–343.
- Kaufhold, S., Dohrmann, R., Sandén, T., Sellin, P., and Svensson, D. (2013) Mineralogical investigations of the alternative buffer material test – I. Alteration of bentonites. *Clay Minerals*, **48**, 199–213.
- Kaufhold, S., Sanders, D., Dohrmann, R., and Hassel, A.-W. (2015) Fe corrosion in contact with bentonites. *Journal of Hazardous Materials*, **285**, 464–473.
- Kaufhold S., Dohrmann R., and Ufer, K. (2016). Interaction of magnesium cations with dioctahedral smectites under HLRW repository conditions. *Clays and Clay Minerals*, **64**, 743–752.
- Karnland, O., Olsson, S., and Nilsson, U. (2007) *Mineralogy and Sealing Properties of Various Bentonites and Smectite-rich Clay Materials*. SKB technical report, TR 06-30. Available online at: <http://www.skb.se/upload/publications/pdf/TR-06-30.pdf>.
- Karnland, O., Olsson, S., Dueck, A., Birgersson, M., Nilsson, U., Hernan-Håkansson, T., Pedersen, K., Nilsson, S., Eriksen, T.E., and Rosborg, B. (2009) Long term test of buffer material at the Äspö Hard Rock Laboratory, MX80 (LOT) project - *Final report on the A2 test parcel*. Technical Report TR-09-29. Available online at: <http://www.skb.se/upload/publications/pdf/TR-09-29.pdf>.
- Kumpulainen, S. and Kiviranta, L. (2011) Mineralogical, chemical and physical study of potential buffer and backfill materials from ABM test package 1. Posiva Working report 2011 – 41. Available online at: http://www.iaea.org/inis/collection/NCLCollectionStore/_Public/43/068/43068661.pdf.
- Kumpulainen, S., Kiviranta, L., and Korkeakoski, P. (2016) Long-term effects of Fe-heater and Äspö groundwater on smectite clays – Chemical and hydromechanical results from *in-situ* alternative buffer material (ABM) test package 2. *Clay Minerals*, **51**, 129–144.
- Lantenois, S., Lanson, B., Muller, F., Bauer, A., Jullien, M., and Plançon, A. (2005) Experimental study of smectite interaction with metal Fe at low temperature: 1. Smectite destabilization. *Clays and Clay Minerals*, **53**, 597–612.
- Mosser-Ruck, R., Pironon, J., Cathelineau, M., and Trouiller, A. (2001) Experimental illitization of smectite in a K-rich solution. *European Journal of Mineralogy*, **13**, 829–840.
- Osacký, M., Šucha, V., A. Czimerová, A., and Madejová, J. (2010) Reaction of smectites with iron in a nitrogen atmosphere at 75°C. *Applied Clay Science*, **50**, 237–244.
- Plötze, M., Kahr, G., Dohrmann, R., and Weber, H. (2007) Hydro-mechanical, geochemical and mineralogical characteristics of the bentonite buffer in a heater experiment. The HE-B project at the Mont Terri rock laboratory. *Physics and Chemistry of the Earth*, **32**, 730–740.
- Pusch, R., Börgesson, L., Fredriksson, A., Johannesson, L.-E., Hökmark, H., Karnland, O., and Sandén, T. (1995) *The Buffer and Backfill Handbook*. Technical Report 95-45, SKB, Clay Technology AB, Sweden.
- Samper, J., Naves, A., Montenegro, L., and Mon, A. 2016. Reactive transport modelling of the long-term interactions of corrosion products and compacted bentonite in a HLW repository in granite: Uncertainties and relevance for performance assessment. *Applied Geochemistry*, **67**, 42–51.
- Sellin, P. and Leupin, O. (2014) The use of clay as an engineered barrier 1 in radioactive waste management – a review. *Clays and Clay Minerals*, **61**, 477–498.
- Sena, C., Salas, J., and Arcos, D. (2010) Thermo-hydro-geochemical modelling of the bentonite buffer LOT A2 experiment. Technical Report TR-10-65. Available online at: http://www.iaea.org/inis/collection/NCLCollectionStore/_Public/42/109/42109942.pdf.
- Svensson, D., Dueck, A., Olsson, S., Sandén, T., Lydmark, S., Jägerwall, S., Pedersen, K., and Hansen, S. (2011) *Alternative Buffer Material – Status of Ongoing Laboratory Investigations of Reference Materials and Test Package 1*. – SKB Technical report TR-11-06. Available online at: <http://www.skb.se/upload/publications/pdf/TR-11-06.pdf>.
- Svensson, D. (2013) Early observations in a large scale 6½ year iron-bentonite field experiment (ABM2) at Äspö hard rock laboratory, Sweden. *50th Annual Meeting of The Clay*

- Minerals Society, October 6-10. Urbana-Champaign, Illinois, U.S.A., Abstracts*, 233-244.
- Svensson, D. and Hansen, S. (2013) Redox chemistry in two iron-bentonite field experiments at Äspö Hard Rock Laboratory, Sweden: An XRD and Fe K-edge XANES study. *Clays and Clay Minerals*, **61**, 566–579.
- Svensson, D. (2015) Saponite formation in the ABM2 iron-bentonite field experiment at Äspö hard rock laboratory, Sweden. *Clays in Natural and Engineered Barriers for Radioactive Waste Confinement, 6th International Conference, Brussels, March 23–26*.
- Wallis, I., Idiart, A., Dohrmann, R., and Post, V. 2016. The ABM1 test – a reactive transport model of the influence of groundwater on the CEC distribution in bentonite clays. *Applied Geochemistry*, **73**, 59–69.
- Wersin, P., Jenni, A., and Mäder, U.K. (2015) Interaction of corroding iron with bentonite in the ABM1 experiment at Äspö, Sweden: a microscopic approach. *Clays and Clay Minerals*, **63**, 51–58.
- Wilson, J., Savage, D., Cuadros, J., Shibata, M., and Ragnarsdottir, K.V. (2006a) The effect of iron on montmorillonite stability. (I) Background and thermodynamic considerations. *Geochimica et Cosmochimica Acta*, **70**, 306–322.
- Wilson, J., Cressey, G., Cressey, B., Cuadros, J., Ragnarsdottir, K.V., Savage, D., and Shibata, M. (2006b) The effect of iron on montmorillonite stability. (II) Experimental investigation. *Geochimica et Cosmochimica Acta*, **70**, 323–336.

(Received 27 October 2016; revised 15 February 2017; Ms. 1146; M. Plötze)